



**HAL**  
open science

# Cimmerian block detachment from Gondwana: a slab pull origin ?

Tiphaine Larvet, Laetitia Le Pourhiet, Philippe Agard

► **To cite this version:**

Tiphaine Larvet, Laetitia Le Pourhiet, Philippe Agard. Cimmerian block detachment from Gondwana: a slab pull origin ?. *Earth and Planetary Science Letters*, 2022, 596, 10.1016/j.epsl.2022.117790 . hal-03787010

**HAL Id: hal-03787010**

**<https://hal.science/hal-03787010>**

Submitted on 23 Sep 2022

**HAL** is a multi-disciplinary open access archive for the deposit and dissemination of scientific research documents, whether they are published or not. The documents may come from teaching and research institutions in France or abroad, or from public or private research centers.

L'archive ouverte pluridisciplinaire **HAL**, est destinée au dépôt et à la diffusion de documents scientifiques de niveau recherche, publiés ou non, émanant des établissements d'enseignement et de recherche français ou étrangers, des laboratoires publics ou privés.

# Cimmerian block detachment from Gondwana: a slab pull origin ?

Tiphaine Larvet<sup>a,\*</sup>, Laetitia Le Pourhiet<sup>a</sup>, Philippe Agard<sup>a</sup>

<sup>a</sup>*Institut des Sciences de la Terre de Paris (ISTeP), Sorbonne Université, Paris, France*

---

## Abstract

The Cimmerian blocks are ribbons-like micro-continents that detached from the northern margin of Gondwana during the closure of the Paleotethys ocean at the end of the Permian. While it has been hypothesized that slab pull forces induced by subduction of the Paleotethys beneath Eurasia could have driven extension in the lower plate after the Paleotethys mid-oceanic ridge subduction, so far, numerical modelling studies have concluded that these forces alone are not sufficient to drive continental breakup. However, the previous modelling studies neglects olivine phase transitions in the mantle and likely underestimated the slab pull. Here, we present numerical simulations that consider the evolution of the density of the slab associated with metamorphic reactions and analyze carefully when, where, and how the slab pull can lead to the formation of micro-continents. Our results show that the marked increase in slab density related to olivine phase transitions at 410 km discontinuity, in addition to gravitational potential energy, can cause continental rifting of the lower plate. Nonetheless, continental breakup is only achieved in absence of horizontal shear flow at the base of the continental lithosphere. In these successful experiments, the deformation localizes 100-200 km on shore due to bending stress pointing out that this process probably always leads to the formation of small continental ribbons. Our results confirm that the tensional force induced by the Paleotethys subduction dynamics may have caused the detachment of the Cimmerian blocks. Since continental breakup of the lower plate is promoted in the absence of basal shear below Gondwana's lithosphere (with respect to the underlying mantle), we argue that the formation of the Cimmerian blocks provides information on the relative motion between the tectonic plates and the underlying mantle. Our simulations demonstrate that there is a significant time-lag between ridge subduction and continental breakup (i.e. the time needed for the slab to reach the 410 km discontinuity), which is rarely accounted by paleogeographic reconstructions.

---

\*corresponding author: [tiphaine.larvet@sorbonne-universite.fr](mailto:tiphaine.larvet@sorbonne-universite.fr), 4 place jussieu, 75005, France

*Keywords:* Numerical model, Subduction, Continental breakup, Slab pull, Neotethys, Cimmerian blocks

---

## 1. Introduction

The breakup and reassembly of super-continent is a cyclic mechanism that dominates plate tectonics throughout Earth's life, with continental blocks detaching and drifting in response to the openings and closings of oceanic domains. Why and how continental breakup occurred is still poorly understood. One class of models requires the coupling of deep subduction, mantle flow and continental thermal blanketing to form large continental landmass (Dal Zilio et al., 2018; Jolivet et al., 2016; Heron, 2019; Guillou and Jaupart, 1995). The second class addresses the formation of smaller continental fragments and relies on localised pull forces with the help of intervening plumes (Stampfli and Borel, 2002; Müller et al., 2001; Gerya and Meilick, 2011; Koptev et al., 2019; Lavecchia et al., 2017).

A particular feature arises, however, when continental breakup affects the passive margin selectively, leading to the formation of a series of relatively linear microcontinents. Such was the case of the Cimmerian blocks, a  $> 3000$  km long and generally  $< 500$  km wide ring of continental fragments, which detached from the Gondwana margin during the Permian and drifted northward until they collided with Eurasia in the early Triassic (Fig.1A; Ricou 1994; Agard et al. 2011). While this process relates to the northward subduction of the Paleotethys ocean beneath Eurasia (Ricou, 1994; Agard et al., 2011). Two main conceptual models have been proposed to explain their formation: a plume-induced continental breakup model and a subduction related continental breakup model (Fig. 1B).

Plume-induced microcontinent formation has been proposed for the formation of small, isolated, rounded microcontinents (i.e. the Seychelles, Jan Mayen, and eastern Tasmanian Plateau) in a tensional tectonic framework (Müller et al., 2001). In this scenario, a plume beneath the passive margin causes the emplacement of LIPs at the surface. At depth, the heat from the plume leads to a local decrease in lithospheric strength, resulting in continental rifting, breakup and, ultimately, the jump from the mid-ocean ridge (Müller et al., 2001). The continental rifting and breakup by jumping of the mid-ocean ridge beneath the plume have been successfully reproduced by numerical modeling studies with divergent plate boundary conditions (Lavecchia et al., 2017).

In contrast, the slab pull related continental breakup model (Stampfli and Borel, 2002; Wan et al., 2019) assumes that slab pull becomes strong enough, after subduction of the mid-oceanic ridge, to detach the passive margin from the continent and create a new spreading center in between. Contrary to the plume-induced continental breakup model, the slab pull one does not require far field divergence since the

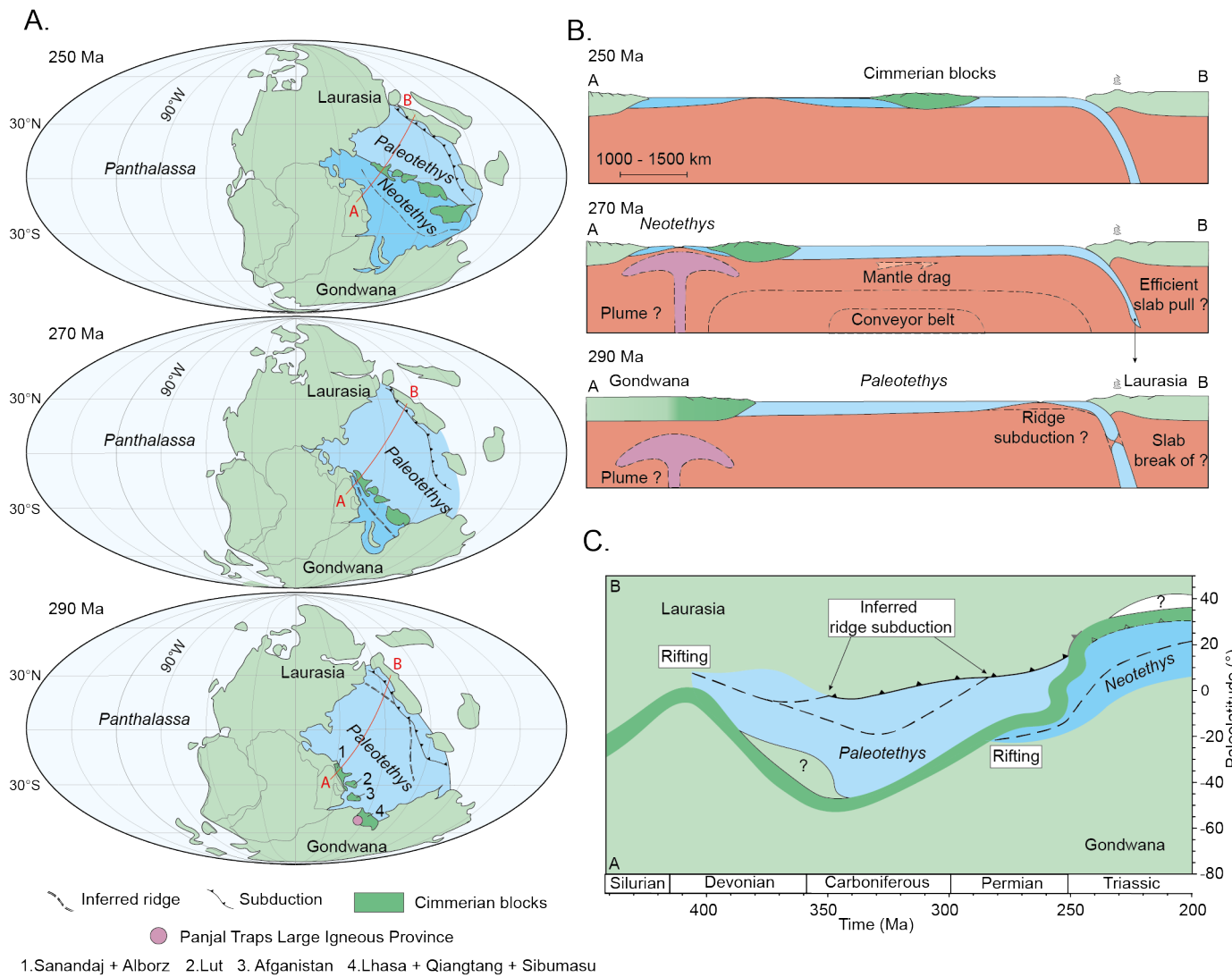


Figure 1: A. Paleogeographic reconstruction from early Permian to early Triassic, modified from Torsvik and Cocks (2016). The red trace indicates the position of the schematic evolutions shown in B. B. Schematic geodynamic cross-section showing a tentative explanation for the detachment of the Cimmerian blocks, emphasizing the role of various potential mechanisms. C. Location of the Cimmerian microcontinents and oceanic domains through time (paleolatitude data from Muttoni et al. (2009)). Inferred ridges are shown as dashed lines. Two hypotheses are presented: ridge subduction long before the Neotethys rifting (Wan et al., 2021) or just before (Torsvik and Cocks, 2016).

extensional regime is inherently generated by the subduction process. However, this conceptual model has not yet been successfully reproduced by numerical modelling. One existing study concluded to the need of an inherited weakness to lead to continental margin breakup (Yang et al., 2021), whereas the second one concluded to the need of a plume beneath the margin (Koptev et al., 2019), in addition to slab-pull forces. In the latter interpretation, the successive detachment and drift of micro-continents in the Tethyan domain (i.e. the Cimmerian blocks in the Permian, the Apulia micro-continent in the Triassic, and the Arabic micro-continent in the Cretaceous) would be the result of a hybrid process requiring the coincidental persistence of a super-plume under the Tethyan margin since the Paleozoic, combined with the "slab-drag" of the Paleotethys and then of the Neotethys (Torsvik et al., 2012; Jolivet et al., 2016).

A common limitation of the two previous numerical studies exploring the slab-drag model is that they strongly underestimated the slab pull force. One study was indeed bounded to 200 km depth (Koptev et al., 2019), while the other neglected the metamorphic reactions and the gradual density increase associated with plate burial (Yang et al., 2021), all of which strongly hampers the full development of slab pull force to drag the plate. This work therefore uses more realistic estimates of the buoyancy and force balance to test if the slab pull alone is sufficient to rip the Cimmerian blocks away for the Gondwana margin. We then discuss the geodynamic significance of the conditions necessary for this slab pull related continental breakup to occur, as well as the timing between mid-ocean ridge subduction and micro-continent formation (Fig. 1C)

## 2. Method

The simulations are carried out with pTatin2D (May et al., 2014, 2015), a software package designed to study long time-scale processes relevant to geodynamics. It has been widely used and validated for intraplate deformation case studies in former publications (e.g. Jourdon et al. 2018; Le Pourhiet et al. 2018; Jourdon et al. 2020). This study presents its first application to subduction zones for which we have implemented mineral transformations through look-up table for density changes and variable melting proportions. The description of the computational method can be found in (May et al., 2014, 2015). In this part, we briefly present the key equations and focus on the presentation of the setup.

### 2.1. Governing equation

pTatin2D is a thermo-mechanical code based on the finite element method using an arbitrary Lagrangian-Eulerian grid coupled with material point method. The pressure and velocity are predicted by solving conservation of mass

$$\nabla \cdot \mathbf{v} = 0 \tag{1}$$

and momentum

$$\nabla \cdot \eta (\nabla \mathbf{v} + (\nabla \mathbf{v})^t) - \nabla P + \rho \mathbf{g} = 0 \quad (2)$$

for an incompressible fluid under the Boussinesq approximation. In equation 2,  $\eta$  stands for the effective viscosity,  $\mathbf{v}$  for the velocity vector,  $P$  for the pressure,  $\mathbf{g}$  for the gravity acceleration vector and  $\rho$  for the density of the material. This system of equation is coupled with the energy conservation equation,

$$\frac{\partial T}{\partial t} = -\nabla \cdot (-\kappa \nabla T + \mathbf{v}T) + \frac{H}{\rho cp}, \quad (3)$$

where  $T$  corresponds to the temperature,  $\kappa$  the thermal diffusivity ( $10^{-6} m^2/s$ ),  $cp$  the heat capacity and  $H$  the heat production. The viscosity ( $\eta_v$ ) is obtained by harmonic averaging

$$\frac{1}{\eta_v} = \frac{1}{2} \left( \frac{1}{\eta_{ds}} + \frac{1}{\eta_{df}} \right), \quad (4)$$

of viscosity ( $\eta_{ds}$ ) predicted by dislocation creep

$$\eta_{ds} = A_{ds}^{-\frac{1}{n}} (\dot{\epsilon}^{II})^{\frac{1}{n}-1} e^{\frac{Q_{ds} + PV_{ds}}{nRT}} \quad (5)$$

and the viscosity ( $\eta_{df}$ ) predicted by diffusion creep

$$\eta_{df} = A_{df}^{-1} e^{\frac{Q_{df} + PV_{df}}{RT}}. \quad (6)$$

In equation 5 and 6,  $\dot{\epsilon}^{II}$  stands for the second invariant of the strain rate tensor,  $A$  is the pre-exponential factor,  $n$  is the stress exponent,  $Q$  is the activation energy and  $V$  the activation volume (Tab1). When the stress exceeds either a frictional limit set by the Drucker-Prager yield criterion ( $\sigma_{DP}$ )

$$\sigma_{DP} = C \cos \phi + P \sin \phi, \quad (7)$$

which depends on cohesion ( $C$ ) and friction angle ( $\phi$ ), or a maximum strength ( $\sigma_{max}$ ), the viscosity is corrected according to

$$\eta = \min \left( \eta_v, \frac{\sigma_{max}}{2\dot{\epsilon}^{II}}, \frac{\sigma_{DP}}{2\dot{\epsilon}^{II}} \right). \quad (8)$$

Finally, cohesion and friction angle decrease linearly with plastic strain ( $\varepsilon_p$ ) in the range  $[\varepsilon_{min}, \varepsilon_{max}]$  according to

$$\phi = \phi_0 - \frac{\varepsilon_p - \varepsilon_{min}}{\varepsilon_{max} - \varepsilon_{min}} (\phi_0 - \phi_\infty), \quad (9)$$

	Sediment (Wet quartzite (Gleason and Tullis, 1995))	Oceanic crust (Diabase (Burov and Guillou- Frottier, 1999))	Continental upper crust(Dry quartzite (Ranalli and Murphy, 1987)	Continental lower crust (Wet quartzite (Turcotte and Schubert, 2014))	Upper mantle (Dry Olivine (van Hunen et al., 2000))	Lower mantle (Dry Olivine (van Hunen et al., 2000)(Čížková et al., 2012))	Weak zone (Dry Olivine (van Hunen et al., 2000))
Friction							
$C_0 - C_\infty$ (MPa)	2 <sup>a</sup> -1	2-1	20-2	20-2	20-2	20-2	1-1
$\phi_0 - \phi_\infty$ (°)	2 - 0.1	2-0.1	20-10	20-10	20-10	20-10	0.1-0.1
$\varepsilon_{min} - \varepsilon_{max}$	0.5 - 2	0.5 - 2	0.5 - 2	0.5 - 2	0.5 - 2	0.5 - 2	0.5 - 2
Pseudo-plasticity							
$\sigma_{max}$ (MPa)	200	200	400	400	200-400 <sup>b</sup>	400	400
Dislocation							
$n$	4.00	3.05	2.40	2.60	3.50	3.50	3.50
$A_{ds}$ ( $Pa^{-n} s^{-1}$ )	1.1 x10 <sup>-28</sup>	6.31 x10 <sup>-20</sup>	2.5x10 <sup>-20</sup>	1.1x10 <sup>-17</sup>	2.42 x10 <sup>-16</sup>	2.42 x10 <sup>-16</sup>	2.42 x10 <sup>-16</sup>
$Q_{ds}$ ( $Jmol^{-1}$ )	2.23 x10 <sup>5</sup>	2.76 x10 <sup>5</sup>	1.56 x10 <sup>5</sup>	2.30 x10 <sup>5</sup>	5.40 x10 <sup>5</sup>	5.40 x10 <sup>5</sup>	5.40 x10 <sup>5</sup>
$V_{ds}$ ( $m^3mol^{-1}$ )	10x10 <sup>-6</sup>	10x10 <sup>-6</sup>	10x10 <sup>-6</sup>	10x10 <sup>-6</sup>	14x10 <sup>-6</sup>	20x10 <sup>-6</sup>	10x10 <sup>-6</sup>
Diffusion							
$A_{df}$ ( $Pa s^{-1}$ )					1.92x10 <sup>-11</sup>	1.3x10 <sup>-17</sup>	
$Q_{df}$ ( $Jmol^{-1}$ )					3.00 x10 <sup>5</sup>	2.00x10 <sup>5</sup>	
$V_{df}$ ( $m^3mol^{-1}$ )					4.5x10 <sup>-6</sup>	1.1x10 <sup>-6</sup>	

Table 1: Rheological Parameters. <sup>a</sup> Sediments coming from topography erosion during the simulation are considered unconsolidated, they have a initial frictional angle of 1°. <sup>b</sup> The oceanic lithosphere maximal stress is set at 200 MPa. The rest of the mantle have a 400 MPa maximal stress

here given for friction. Rheological parameters, specific to each rock type, are detailed in Table 1.

## 2.2. Metamorphic reactions and density

Considering that the slab pull force is the main driver of the subduction dynamics, density prediction is essential in our simulations. To model the evolution of density as accurately as possible, we implemented precomputed rock density look-up tables (Fig.2; Gerya et al. (2001, 2004); Vasilyev et al. (2004)). The density of rocks depends on the constitutive minerals ( $i$ ), their proportion ( $N_i$ ), their density ( $\rho_i$ ) and on

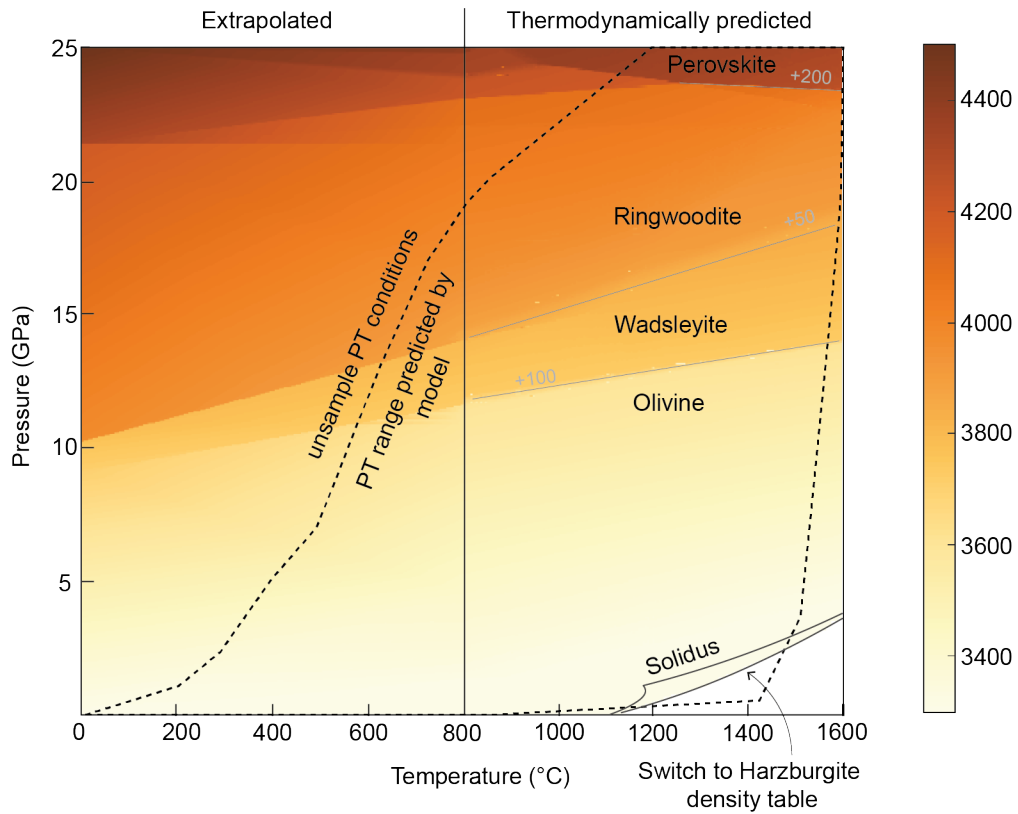


Figure 2: Density table for Lherzolite composition showing the density jump associated with the olivine polymorphic reaction. The dashed line represents PT conditions extracted from the numerical simulations. Mantle densities are thermodynamically predicted above 800°C. Densities are extrapolated at lower temperatures, since solid solution models are not available and the assumption of equilibrium is less robust. At low pressure and high temperature conditions, the bulk rock composition is corrected after 22% of melting.

Pressure and Temperature (PT) conditions:

$$\rho_{(P,T)} = \sum_{i=1}^n \rho_{i(P,T)} N_{i(P,T)} \quad (10)$$

Stable phase assemblages have been predicted using the thermodynamic software `Perple_X` which minimizes the free Gibbs energy according to PT conditions, for any given bulk rock chemistry composition. In order to encompass the diversity of material in the slab, three different bulk rock compositions were considered: a mafic composition for the oceanic crust, a K-Al-rich composition representative of continent-derived material and an ultramafic composition for mantle rocks (Fig.2). In order to cover the entire PT range of possible thermo-mechanical simulations, even in regions out of reach for thermodynamic calculation and/or equilibrium (i.e. where solid solution models are not available or at too low temperature), densities are extrapolated using the closest computed density, the thermal dilatation ( $\alpha$ ) and the elastic compressibility ( $\beta$ ):

$$\rho_{(P,T)} = \rho_{(P_0,T_0)}(1 - \alpha(T - T_0) + \beta(P - P_0)) \quad (11)$$

`Perple_X` also predict a melt phase. In the simulation, we consider that the melt is extracted as soon as it forms and causes no rheological weakening nor buoyancy effect. Yet the density and buoyancy of the rocks do change through changes in composition. Moreover, as `Perple_X` is based on the assumption of a chemically closed system, the neglect of the progressive depletion of the source rock in incompatible elements leads to an overestimation of melt proportion in the pre-computed table. It is not computationally tractable to call `Perple_X` at every time step. Here, we attempt a rough approximation which consists at changing the bulk rock composition after a critical melt fraction has been reached. These critical melt fraction depends on the mineralogy. For mantle rocks, the composition is corrected after 22% of melting, which corresponds to the breakdown of clinopyroxene. For continental and oceanic rocks, we use the breakdown of hydrous minerals, respectively white mica (after 34% of melting) and amphibole (after 18% of melting). In practice, we just switch from the initial look-up table to a new look-up table computed with the residual material composition (Fig.2). We also warn the reader that the presence of water is taken into account for oceanic crust and continental affinity material, but neglected for mantle calculations. In consequence, only adiabatic melting is simulated in this study. The interested reader will find detailed calculation of look-up tables, including the bulk composition for each rock type and the list of solid solution models in the supplementary material.

### 2.3. Model set up

The domain is 4000 km-long and 900 km deep (Fig.3). On the left side, the initial compositional structure accounts for a 500 km-long continental domain which represents the edge of Gondwana and its passive margin. This continent is attached to a 2000 km-long oceanic domain which represents the Paleotethys after the subduction of the mid-oceanic ridge and the detachment of the slab (Burkett and Billen, 2009). On the right side, a 1500 km-long continental domain simulates Eurasia. Between the lower plate and the upper plate, a 10 km-thick zone with low friction material is added to provide initial decoupling between the tectonic plates and to initiate subduction. The grid is subdivided into 384 by 96 Q2 elements (nine-nodes quadrilateral element) and refined with a maximum resolution of 6.5 by 5 km along the subduction interface. The oceanic plate is made of 4 km of sediment over 7 km of mafic crust and the continental crust is composed of 20 km of upper crust and 16 km of lower crust (Fig.3a). The oceanic lithosphere geotherm follows a plate cooling model (Turcotte and Schubert, 2014) with a constant age of 30 Ma:

$$T_{oce} = T_l \left[ \frac{y}{yl} + \frac{2}{\pi} \sum_{i=1}^{150} \frac{1}{n} e \left( -\frac{\kappa n^2 \pi^2 t}{yl^2} \right) \sin \left( \frac{n\pi y}{yl} \right) \right] \quad (12)$$

where  $T_l$  is the temperature of the lithosphere-asthenosphere boundary (LAB; 1300°C) and  $y_l$  the depth from which the plate stops thickening (95 km depth). Since the northern margin of Gondwana was impacted by the south-dipping Prototethys subduction and the formation of the Paleotethys ocean during the Paleozoic (Stampfli and Borel, 2002), we consider it as a mobile belt at the start of our simulations (i.e. at the end of the Palaeozoic). We define the thermal structure of the continent by setting the surface temperature at 0°, the lithosphere-asthenosphere boundary at 1300°C and a radiogenic heat production decreasing exponentially with depth (Stüwe et al., 2002).

$$T_{cont} = \frac{yT_l}{yl} + \frac{h_r^r S_0}{k} \left( (1 - e^{-\frac{y}{h_r}}) - (1 - e^{-\frac{y_l}{h_r}}) \frac{y}{yl} \right) \quad (13)$$

where  $k$  is the thermal conductivity ( $3 \text{ Js}^{-2} \text{ m}^{-1} \text{ K}^{-1}$ ) and  $h_r$  is the depth of the characteristic drop off (1/e) of heat production, set here at 25 km to reach a MOHO temperature 700°C and to fit the slope of the geotherm for continental region (Artemieva, 2006). The depth of the LAB and the amount of heat production are respectively set at 105 km and  $3 \times 10^{-6} \text{ w/m}^3$ . An adiabatic gradient of 0.5°C/km is imposed below the plates, with  $T = 0^\circ\text{C}$  at the top and  $T = 1700^\circ\text{C}$  at the bottom. The vertical sides are thermally insulated. The top surface is a free surface. At the bottom (900 km depth), the condition is free slip. Our study focuses on subduction within the upper mantle, hence a first-order approximation of a two-order of magnitude

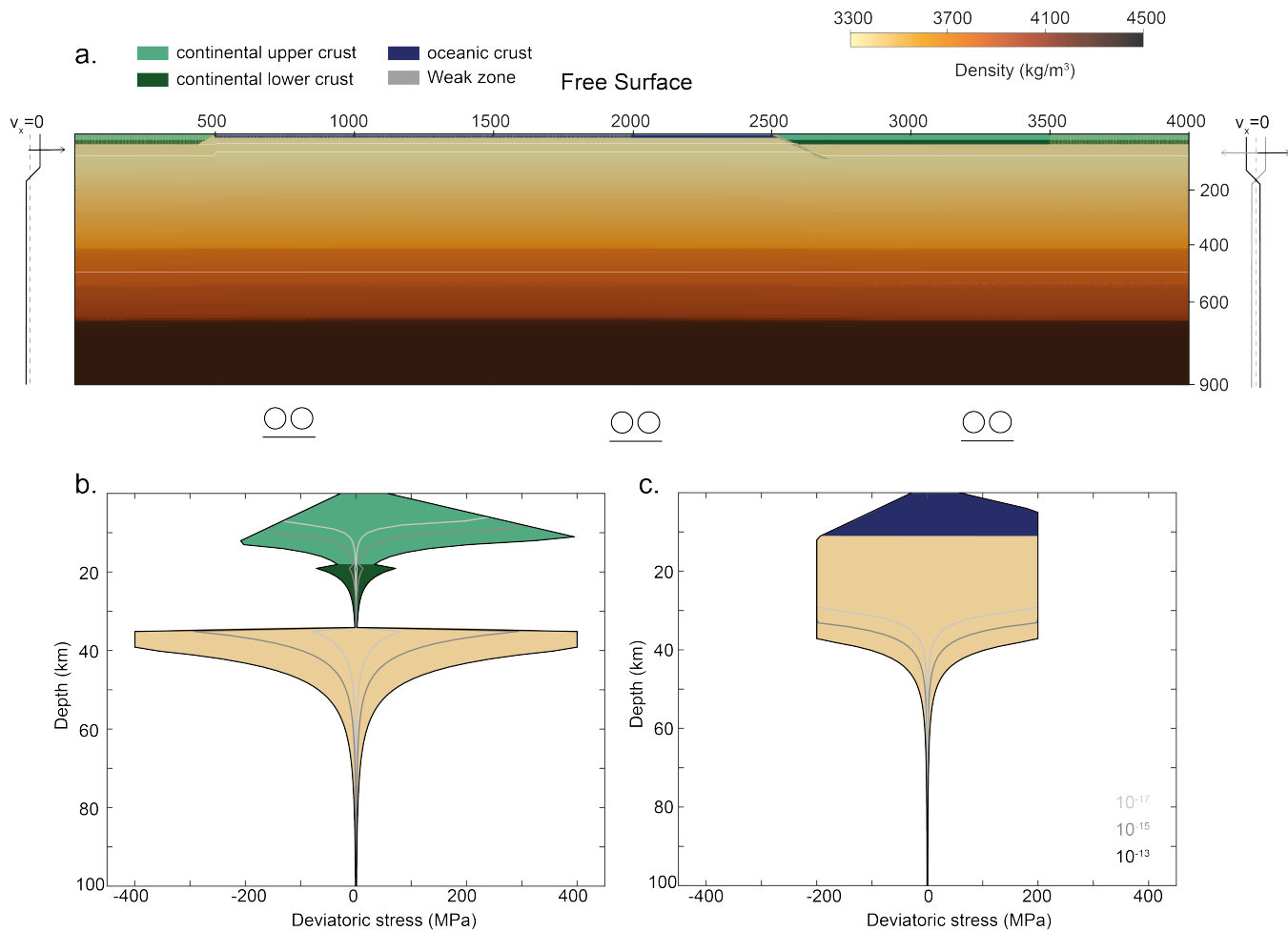


Figure 3: a. Presentation of the initial geometry and boundaries conditions. White lines represent the 700°C, 1100°C and 1500°C isotherms. Continental and oceanic crust are represented in green and blue, respectively. Mantle density is indicated by the orange-brown colors. b and c. Yield strength envelopes of the continent (b.) and the ocean (c) for different values of strain rate.

viscosity contrast between the upper and lower mantle used here is such that the 670 km discontinuity is almost impermeable and act almost as a no slip condition at the 670 km discontinuity. Since the presence of a viscosity jump is debated and is known to feed back on slab dip at depth, two additional simulations have been run with linearly increasing viscosity to validate that our initial and boundary conditions are relevant to discuss continental breakup related to the olivine-wadsleyite transition. Convergence between Gondwana and Eurasia is simulated by injecting continental lithosphere either symmetrically on both sides (Gondwana and Eurasia) or on one of them only. This incoming flow in the lithosphere is compensated at depth by an outflow of asthenosphere (Buiter et al., 2009). The horizontal velocity change with depth is progressive over 40 km depth but yet lead to different intensity of basal shear flow underneath the continent depending on the boundary conditions. The slow paleoconvergence rate between Gondwana and Eurasia during the Permian is inferred from paleomagnetic data. To account for uncertainties between the different studies (Muttoni et al., 2009; Torsvik et al., 2012; Yan et al., 2019), we tested different values of convergence, from 0.5 to 3 cm/year.

### 3. Results

#### 3.1. Evolution of the reference simulation

In order to constrain the relationship between subduction and micro-continent formation we track the density anomaly generated by the slab, expressed as:

$$\Delta\rho_{slab} = \frac{\sum_{S_{slab}} (\rho_{slabcell} - \rho_{mantlecell}) dS_{cell}}{S_{slab}} \quad (14)$$

Material located deeper than 90 km depth and with  $T < 1100^\circ\text{C}$  is herein considered as slab material. We monitor the resulting horizontal force on the lower plate by integrating the horizontal deviatoric stress over a vertical profile extending from the surface to 130 km depth,

$$F_{NSP} = \int_{z=130km}^{z=0km} \sigma_{xx}^d dz, \quad (15)$$

that is located at 100 km from the left boundary of the model. In the reference simulation we impose a constant 2 cm/year convergence rate on the left side of the lower plate. Subduction initiation is forced by the convergence velocity imposed on the continental lithosphere of the lower plate. During this initiation phase, the nascent subduction zone does not yet compensate for the influx of material from the boundary. The difference between the horizontal velocity of the lower plate continent and that of subduction induces overall compressive stress regime (Fig. 4a).

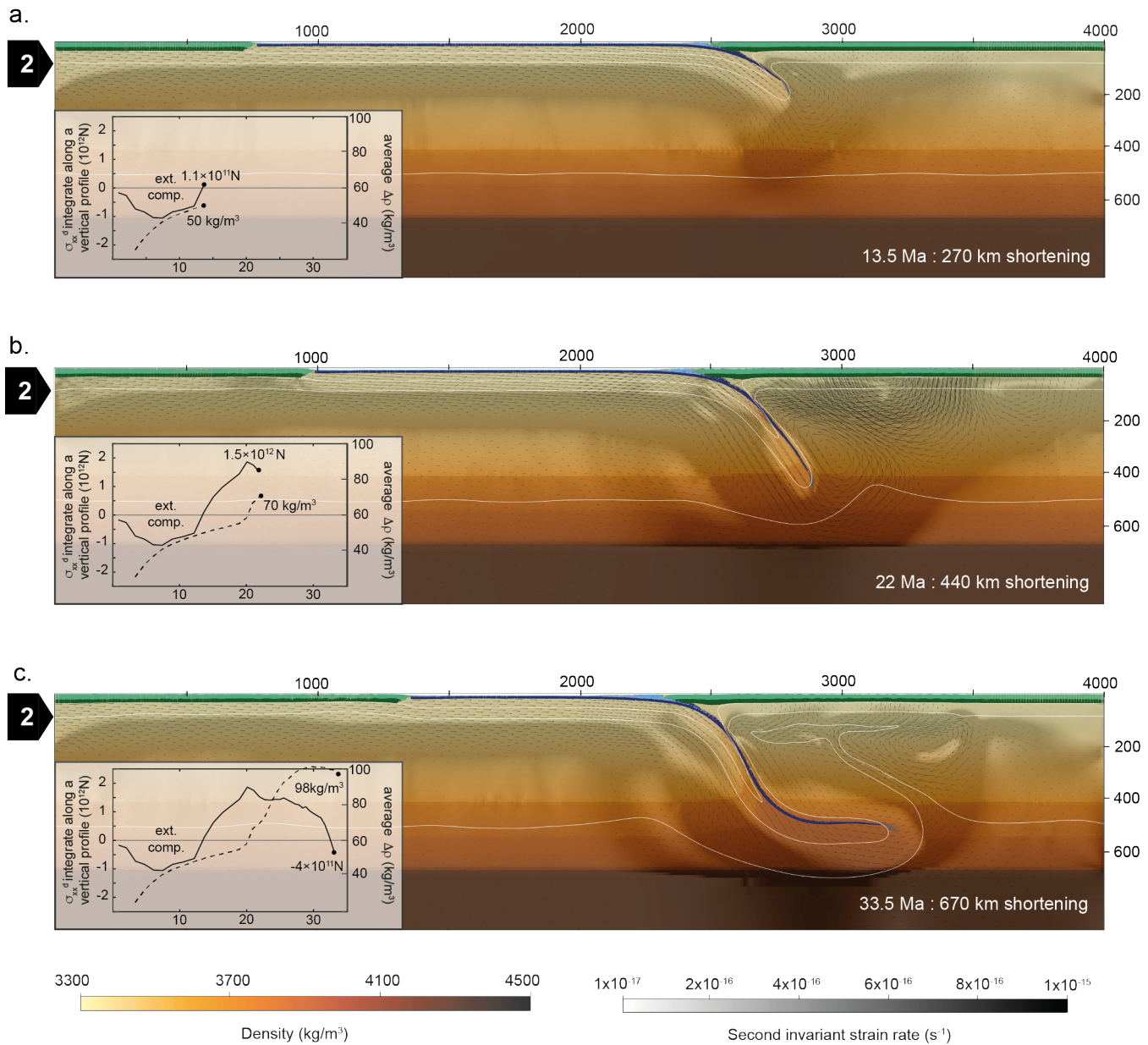


Figure 4: Evolution over time for the reference simulation with a convergence rate of 2 cm/year imposed on the lower plate. Continental and oceanic crust are represented in green and blue, respectively. Mantle density is indicated by the orange-brown colors. Gray overlays are added to highlight deforming areas.

As the slab starts sinking, the difference in density between the slab and the mantle increases and the compressive stress regime affecting the lower plate decreases gradually. After 270 km of shortening, the density contrast between the slab and the surrounding mantle is on average  $50 \text{ kg/m}^3$  (Fig. 4a). This is sufficient to generate a sinking slab velocity equal to or slightly larger than the prescribed convergence rate. Under these boundary conditions, the stress recorded in the lower plate is almost neutral. The lower plate moves like a rigid body and drags the underlying mantle (Fig. 4a). On the upper plate side, subduction leads to the formation of a few hundred km-wide 'corner flow' cell in the mantle wedge. Above this cell, the strength of the plate is reduced in the vicinity of the magmatic arc domain. At 20.5 Ma, the slab crosses the 410 km depth phase transition. Olivine in the slab transforms to wadsleyite and the density contrast between the slab and the surrounding mantle increases drastically ( $70 \text{ kg/m}^3$ ; Fig.4b). The imposed 2 cm/year convergence rate no longer compensates the material entering subduction. The stress regime of the lower plate becomes tensional and the yield strength is reached at the left margin, which starts elongating. A passive upwelling forms below the continental margin to compensate for the thinning of the lithosphere. On the upper plate side, corner flow dynamics become more vigorous. The strength of the upper plate continues to decrease, and the upper plate elongates as a result of slab roll back (Fig.4b). After 33.5 Ma (670 km shortening at the left boundary), the slab starts flattening along the upper-lower mantle boundary (Fig.4b). Slab length is approximately 900 km (i.e. significantly  $> 670$  km of shortening), showing that the lower and upper plates have been elongating collectively by more than 200 km. The density contrast is maximum but the slab is now flattening on the transition zone, which causes a drop in the tensional stress. From there on, corner flow dynamics decrease below the upper plate, plates stop deforming and the trench stops retreating.

This reference model shows that different mechanisms control internal plate deformation. Upper plate extension is promoted by basal thermal erosion related to poloidal mantle flow, whereas lower plate strain depends solely on slab pull. The model also evidences a specific time window during which the slab sinking velocity is maximal, when the slab tip is located between 410 and 670 km depth, leading to optimal conditions for lower plate continental breakup.

### *3.2. Final geometry depending of convergence rates*

Varying systematically the imposed convergence velocity between the two continents and whether convergence is applied on the lower or the upper plate, four distinct deformation modes arise: stable subduction, upper plate continental breakup, lower plate continental breakup and continental breakup of both plates. The relationship between the convergence rate, plate velocity and deformation mode is summarized into a phase diagram in figure 5.

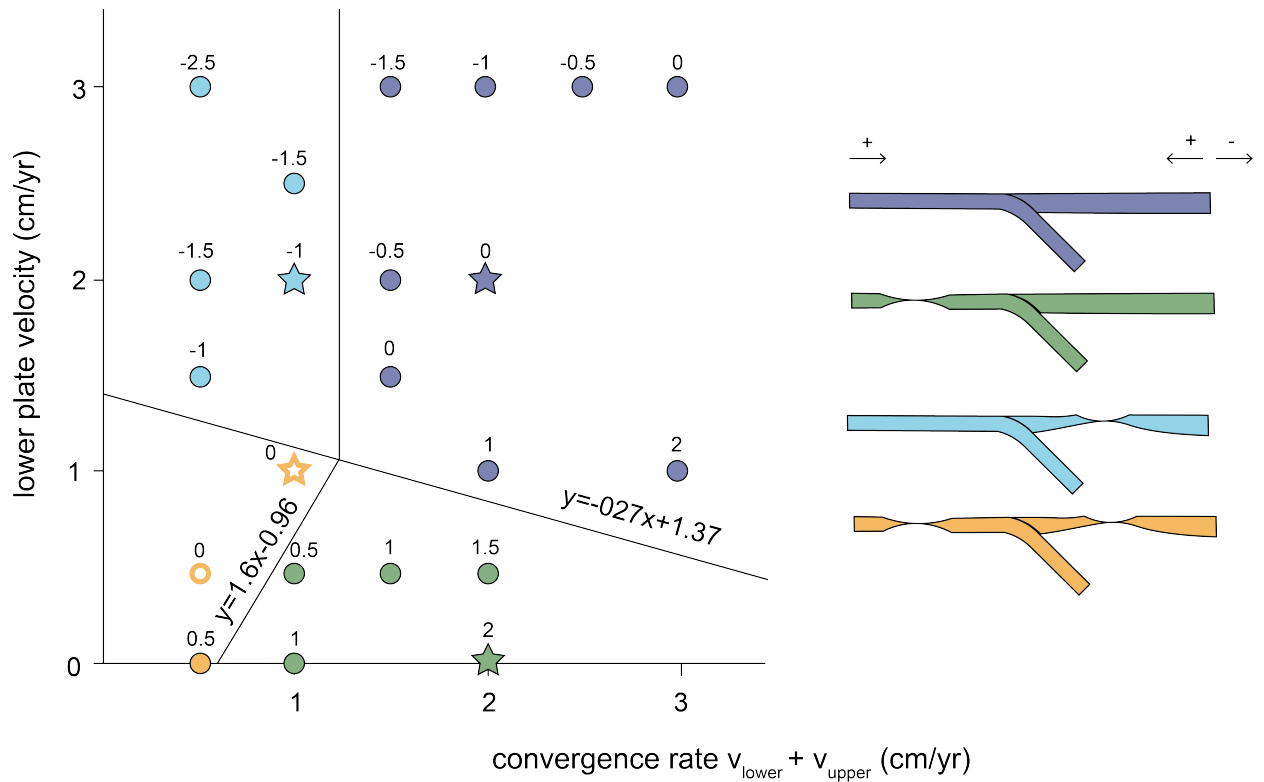
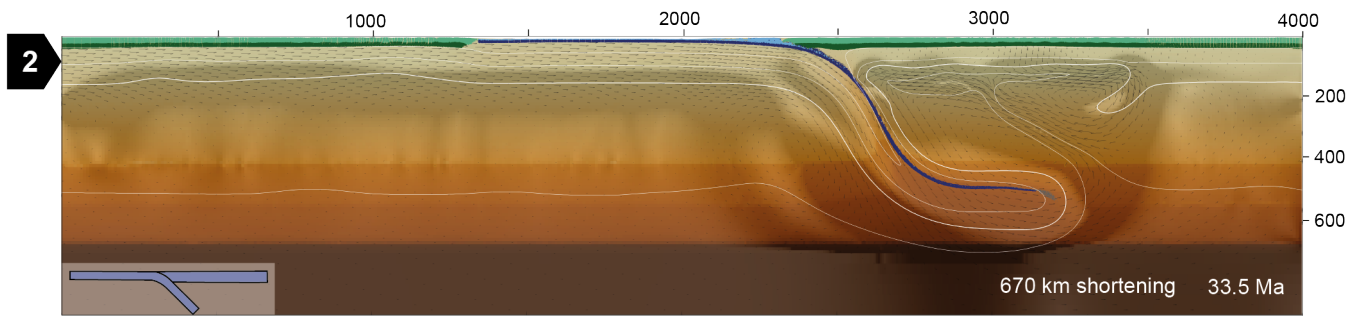
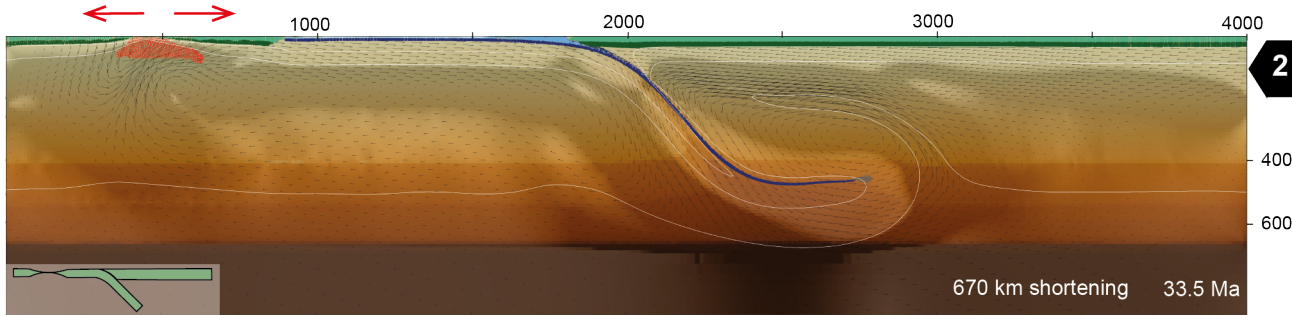


Figure 5: Relationship between the lower plate velocity, total amount of convergence and deformation mode. Numbers keyed to simulations refer to upper plate velocities. Stars outline simulations described in detail in the text. Empty yellow symbols correspond to simulations where rifting starts, yet aborts. Velocities directed towards the subduction zone are shown here as positive.

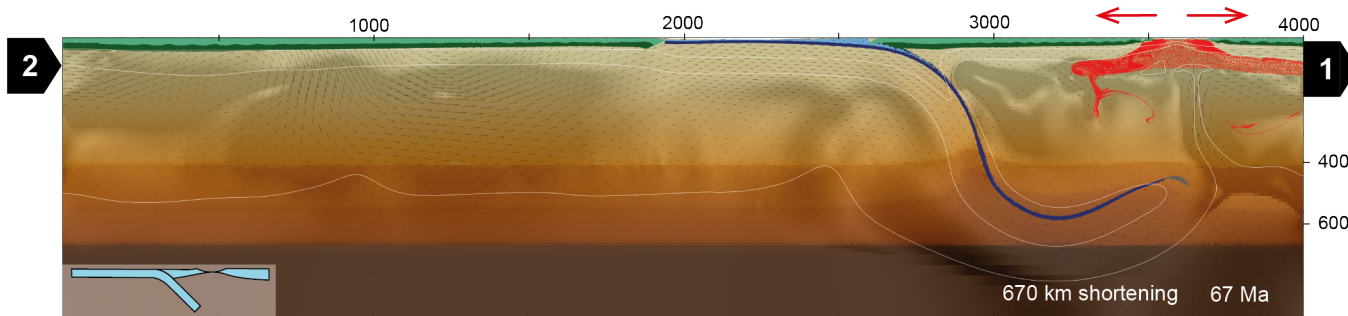
a. Convergence prescribed to the lower plate - No break up



b. Convergence prescribed to the upper plate - Break up of the lower plate



c. Upper plate pulled - Break up of the upper plate



d. Low convergence prescribed to the lower plate - Break up of the lower plate and the upper plate

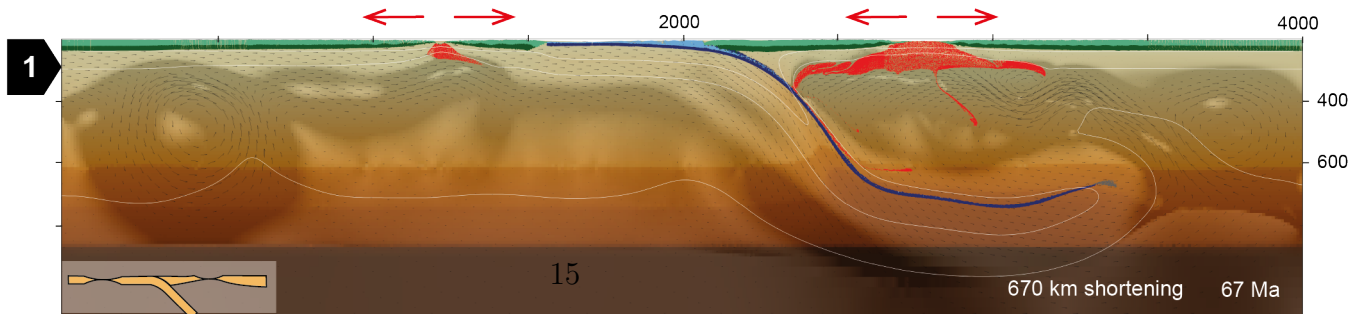


Figure 6: Modes of deformation depending on the amount and direction of convergence imposed to the tectonic plates. Continental and oceanic crust are represented in green and blue, respectively. Mantle density is indicated by the orange-brown colors. Gray overlays are added to highlight deforming areas. The red area represents residue after adiabatic decompression melting which attests for spreading.

A moderate to high lower plate convergence rate ( $\geq 1$  cm/year) generally prevents lower plate continental breakup. If the absolute velocity of the lower plate is high ( $\geq 1.5$  cm/year), the lithosphere of both plates starts thinning but no crustal necking occurs and subduction remains stable (Fig.6a). If the lower plate velocity is sufficiently small ( $< 1$  cm/year), continental rifting occurs in the vicinity of the former passive margin of the lower plate. The rifting stage is followed by continental breakup and by the formation of a spreading center, which leads to the birth of a new ocean (Fig.6b). The lower plate velocity needed to allow for lower plate continental breakup decreases when convergence rate increases (Fig.5). For net convergence rates  $\geq 1.5$  cm/year, upper plate continental breakup is not observed.

Relatively low convergence rates ( $\leq 1$  cm/year) promote continental breakup (Fig.5). When the upper plate is pulled away from the trench (i.e. for upper plate negative velocities; light blue symbols in figure Fig.5 and 6c), only the continent of the upper plate breaks up. In contrast, both continental plates break up when their absolute velocities are both low ( $< 1$  cm/year; Fig. 5d). Depending on whether the lower plate is shear less relatively to the mantle or not, lower plate continental breakup is either followed by oceanic spreading or aborts rapidly (Fig.6b and d). Results show, in general, that continental plates break up either when the plate moves away from the subduction zone, or when the horizontal shear flow imposed at the based of the continental lithosphere by the boundary condition is small.

### *3.3. Spatial distribution and evolution over time of the tensional force*

We monitor the horizontal deviatoric stress using Eq. 15 for four 130 km deep vertical profiles (Fig.7). Their location was chosen so as to avoid local bending, which occurs near the trench and near the continent-ocean transition. Two profiles were chosen 250 km apart for each domain (continental and oceanic). Every profile records the same evolution of the force balance over time: (1) the compressive regime which prevails during the initiation of subduction (2) becomes more and more tensional as the amount of slab material increases (3) until tensional stresses exceed the maximum resistance of the plate and the plate starts to deform; (4) compressive stresses resume once the slab has interacted with the transition zone, partly due to an additional contribution from ridge push. This evolution suggests that deviatoric stresses recorded in the lower plate reflect changes in subduction dynamics. While the force balance evolves similarly in the different profiles (Fig. 7), the differences in absolute values point to the existence of other sources of tensional stresses in addition to slab pull.

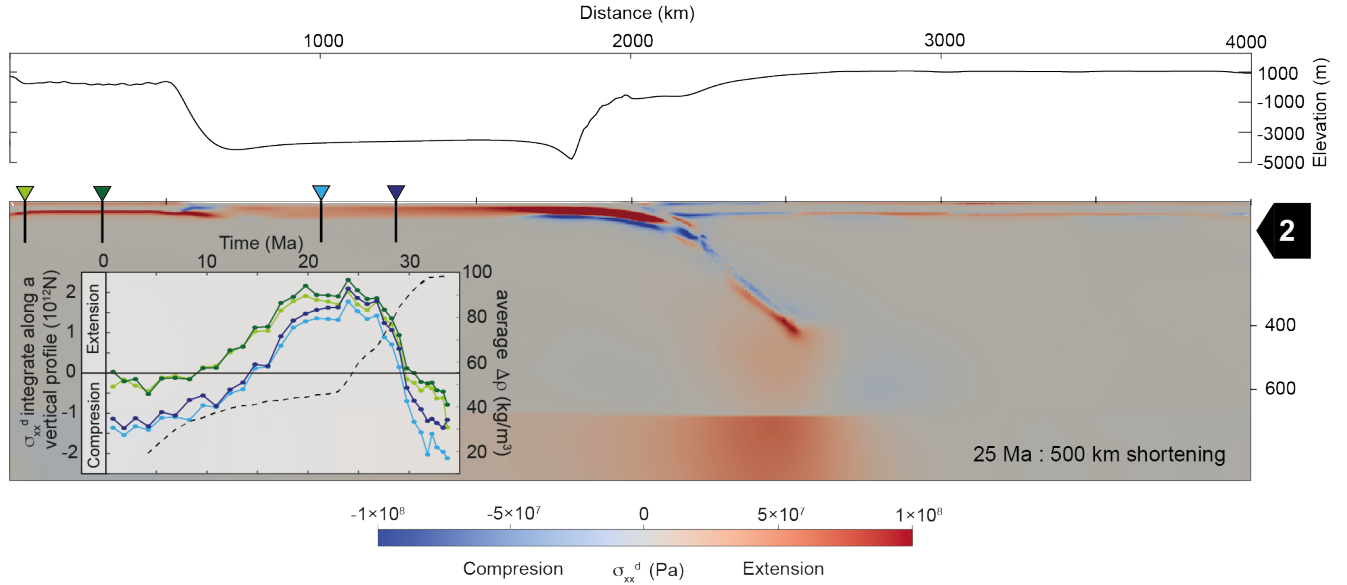


Figure 7: Topographic profile of the simulation at 25 Ma, with 2 cm/year imposed to the upper plate. Deviatoric horizontal stresses are color coded. The evolution of forces acting on the lower plate is shown for four vertical profiles located at 50, 300, 1000 and 1250 km from the left side of the domain.

## 4. Discussion

### 4.1. Opening within the lower plate

In order to break the continent of the lower plate up, the overall force balance of the subduction acting on the lower plate should be equal to or larger than the lower plate strength.

Simulations show that the evolution of forces acting upon the lower plate reflects changes in subduction dynamics (Fig.7). Furthermore, the absolute value of the horizontal tensional deviatoric stress differs as a function of the lateral position of the vertical profile: tensional stresses are always higher (1) in the continent than in the oceanic domain and (2) near the margins. The absolute tensional horizontal stress difference between the continent and the ocean varies with time. At the start of the simulation the tensional stress in the continent edge is about one third higher than in the ocean. When the continent starts thinning, the difference is only one fourth. This evolution correlates with that of elevation throughout the simulation. The elevation difference between the continent and the ocean is about 4700 m at the beginning of the simulation (10 Ma), but decreases to 3900 m at 25 Ma. Hence, we can conclude that the excess of tensional forces in the continent is related to a higher gravitational potential energy (GPE). We also observe a slight difference between profiles in the

same domain yet 250 km apart, with a higher tensional stress near the bending zones. From this, it appears that the GPE and bending forces associated with the ocean-continent transition, though small compared to the slab pull force, also contribute to continental breakup. Since the mass of the slab continues to increase, even after the strength of the plate is reached, it suggests that an even stronger continental margin might break up.

Nevertheless, in this model we neglected two factors that can potentially limited the slab pull force: (1) Metastability is not taken into account in our density table prediction because *Perple\_X* relies on equilibrium thermodynamics. Previous studies have shown that some metastable olivine may remain beyond the equilibrium reaction at 410 km depth, which would reduce the density jump at the 410 discontinuity as well as the increase in slab pull during slab sinking into the upper mantle. However, the maximum extent of olivine metastability is estimated at 500-550 km depth (Faccenda and Dal Zilio, 2017), suggesting that metastable olivine (if any) may delay continental breakup until the slab tip reaches 500-550 km depth but not prevent it. (2) The viscous resistance of the asthenospheric mantle to the horizontal movement of the oceanic lithosphere is likely to dissipate part of the tensional stress generated by the slab pull. Because the viscosity of the top of the asthenospheric mantle is low ( $10^{-19} Pa.s$ ), this basal shear is considered has relatively low. However over long distance it might become important. Paleogeographic restorations indicate a longer Paleotethys ocean during the Permian ( $> 5000$  km). In our model, a 2000 km-long Paleotethys oceanic was considered to avoid high computational cost. To test the impact of a longer Paleotethys domain, an additional simulation was run with a 5000 km-long oceanic domain (see supplementary data). This simulation shows that a longer oceanic domain can somewhat slow down subduction initiation and delay continental breakup but, as for other models, continental breakup occurs once the slab reaches the olivine to wadsleyite transition.

Finally, even if the slab pull force is sufficient to thin continents, continental breakup does not always ensues. Two different deformation patterns have been observed depending on which tectonic plate is moving relative to the underlying asthenosphere. If the lower plate is moving relative to the mantle, deformation is distributed during the entire simulation. In contrast, deformation ultimately localizes near the passive margin if the lower plate is stationary relative to the mantle. Since the stress regime is similar in both cases, this difference in the mechanical response of the lithosphere must be explained by another factor. It has been shown that a horizontal flow passing through an inversely stratified fluid can suppress Rayleigh–Taylor instabilities by delaying their onset and reducing the magnitude of plate-motion-perpendicular convection (Benilov et al., 2002; van Hunen et al., 2003). In the present study, the horizontal flow corresponds to the lower plate on which a convergence is imposed (i.e. Gondwana) and the inversely stratified fluid corresponds to the small scale convection

located below the elongated part of the continental margin during the distributed deformation stage. As the lower plate horizontal velocity is different from the horizontal velocity of the mantle beneath it, the viscous basal shear between them suppresses the perturbation of the LAB caused by rifting. As a result, while the combination of GPE and slab pull force tends to extend the continent, basal shear might delay significantly lithospheric necking. When distributed extension occurs, the thinning of the continental lithosphere results in a decrease of GPE, which in turn reduces the chance of continental lower plate breakup. In the contrary, if the velocities of the continental plate and the asthenosphere mantle below are similar, there is no basal shear and the rifting zone evolves into a localised necking zone.

In order to test if our viscosity jump approximation at the upper to lower mantle transition impacts our results, two additional simulations have been run without viscosity jump at the upper to lower mantle transition (see supplementary movies). The slab flattens due to the positive buoyancy induced by the post-spinel and post-ilmenite endothermic reactions (i.e. with positive Clapeyron slope) which gives the same conclusion: If a velocity is prescribed to the lower plate, the basal shear between the moving tectonic plate and the underlying mantle suppresses the LAB instability and prevents continental breakup. If the convergence is prescribed on the upper plate, then the continent of the lower plate continent breaks up. However, tomography images attest that the slab can penetrate the lower mantle after several tens of thousands to hundreds of millions of years (Goes et al., 2017) of stagnation at the 670 km limit. If the slab penetrates the lower mantle, the slab pull force might evolve. Many factors can affect the slab pull force in the lower mantle. First, the post-garnet reaction that occurs at the top of the lower mantle may lead to an increase in density that could increase the slab pull (Faccenda and Dal Zilio, 2017). On the contrary, the longer the slab stagnates at 670 km, the warmer it becomes and the lower the density contrast between the slab and the mantle. The higher viscosity of the mantle in the lower mantle could, also, further resist slab sinking and reduce the slab pull. However, this viscous resistance depends on the slab surface area which reduces within the lower mantle while the slab tends to become more rounded (Goes et al., 2017). Clearly, more numerical studies are needed to quantify the evolution of slab pull force. That said, if the slab pull force increases during slab sinking into the lower mantle, it is likely to generate continental breakup in the lower plate.

#### *4.2. Comparisons to natural data of subduction zone and previous studies of slab-drag*

The subduction velocity in our simulations varies from a minimum of 0.75 or 1.75 cm/year during the initiation of subduction to a maximum of 5.5 cm/year when the tip of the slab reaches the olivine-wadsleyite transition. Contrary to the initiation stage, during which subduction velocity depends on the imposed far field convergence (e.g. for an imposed 2 cm/year convergence rate, the slab sinks at 1.75 cm/year

whereas, for a 1 cm/year convergence rate, it sinks at 0.75 cm/year), once the slab has reached 410 km its velocity is the same in all simulations where continental breakup occurred. Therefore, except during forced subduction initiation, subduction becomes only driven by buoyancy if continental breakup occurs. In this case, our model predicts a 5 cm/year subduction velocity, consistent with average present-day GPS data for subduction zones (4 cm/year; (Heuret, 2005)).

Models shown here match previous observations linking back-arc formation and upper plate movement with absolute trench motion (Heuret and Lallemand, 2005; Heuret et al., 2007; Lallemand et al., 2008) (Fig.5). Continental breakup of the lower plate is only observed when trench retreat is faster than upper plate trench-ward motion. However, in our simulation, like in others which do not take into account hydration (Wolf and Huismans, 2019), the continental breakup of the upper plate occurs relatively late in the subduction history. Besides, since our 2D numerical models cannot simulate the 3D flow around slab edges, the corner flow below the upper plate expands through time as a result of slab tip migration, such that the basin formation occurs far from the trench. This issue can be solved by implementing progressive slab dehydration into the mantle wedge, which allows for fast weakening of the upper plate near the trench and initiation of back-arc formation during the early subduction stages (Arcay et al., 2008). In our opinion the late occurrence of upper plate continental breakup does not contradict our conclusions on lower continental breakup, because models show that upper plate continental breakup always occurs before the onset of lower plate continental breakup.

Contrary to previous studies which suggested that slab-drag cannot break pristine continental plates (Yang et al., 2021) up, we do observe slab-drag-related continental breakup in our simulation. The major differences between the former models and the present one stem from the incorporation of the thermal effect on density and rheology, the non-linearity of the rheology and the presence of continental crust within the continental plate. Without temperature, the density variation between the slab and the mantle cannot be simulated within the model and must be set as an input parameter. Former studies (Yang et al., 2021; Schellart, 2004) thus postulated a constant slab-mantle density contrast of +80 to +100  $kg/m^3$  for a 80 Ma oceanic plate age. These values are derived from an isostatic analysis of lithospheric buoyancy suggesting that the density contrast between an old lithosphere and the asthenosphere is about 40  $kg/m^3$ , to which about 40  $kg/m^3$  should be added to account for the eclogitization of the oceanic crust during early subduction (Cloos, 1993). This value, however, does not take into account mantle phase transition. In our model, where the density contrast between the slab and the mantle is fully self-consistent, the average contrast of density is 80  $kg/m^3$  for a much younger oceanic lithosphere (30 Ma). In addition, we show that the olivine-wadsleyite reaction is associated with a +50 $kg/m^3$  density contrast between the slab and the mantle and should not be neglected when

simulated slab sinking at more than 410 km depth. Our average continental viscosity under stationary conditions is similar to that of Yang et al. (2021) with respectively  $6.4 \times 10^{23}$  Pa.s and  $7.0 \times 10^{23}$  Pa.s. Yet, the simple temperature-independent used in their study combined with the absence of a continental crust, results in a coupled viscosity profile for the continental plate when our effective results in a decoupled jelly sandwich type profile for the continental plate which is effectively weaker (Burov and Diamant, 1995). Moreover, their study uses linear flow laws which produce slower rate of growth for necking instabilities (Smith, 1977) and temperature independent viscosity and density which are necessary for the transition from passive to active rifting (Huismans et al., 2001). Hence, we argue that even if a simple rheology model (Newtonian, temperature-independent) might be valid for studying subduction dynamics, it is not suitable to study subduction-related continental breakup. The model of Koptev et al. (2019), have all the realistic features (non-linear rheology, thermodynamically consistent density) to simulate continental breakup by slab pull. However, their application domain was restricted to 200 km depth, such that the slab pull force could not fully develop and trigger the lower plate continental breakup without the help of a mantle plume. Yet there is one thing we can learn by comparing their simulation results with ours. In our plume-free model, continental basal shear inhibits necking instability, suggesting that continental breakup only occurs if the plate is not moving relative to the mantle. On the contrary, Koptev et al. (2019) show that continental breakup not only depend on the relative motion between the plate tectonics and the mantle but also to the presence of plume impingement below the continent of the lower plate. Hence, if the lower plate is moving regarding of the underlying mantle, the development of necking instability within the continent of the lower plate is unlikely, except if there is a plume below it

Finally, in our simulations we observe a two-stage rifting, with a first period of slow rifting followed by a fast rifting stage. This result is in agreement with natural observations and a recent analytical and numerical model of rifting (Brune et al., 2016), which emphasizes the importance of using force boundary conditions (as effectively in our model far from model edges) rather than velocity boundary conditions in continental rifting studies. Moreover, we find that the drag exerted by the mantle on the slab limits the extension velocity to 4 or 5 cm/year, corresponding to the cut-off value used in Brune et al. (2016) study to validate their model.

#### *4.3. Implication for the Cimmerian blocks*

This study suggests that the slab pull force, once the slab reaches 410 km depth, together with GPE, is sufficient to break the edge of the Gondwanian continental margin up and detach continental blocks. We also note that the typically 100-200 km-long ribbon-like shape of the Cimmerian blocks (Stampfli and Borel, 2002) agrees better with a process promoting continental breakup as a result of a relatively linear

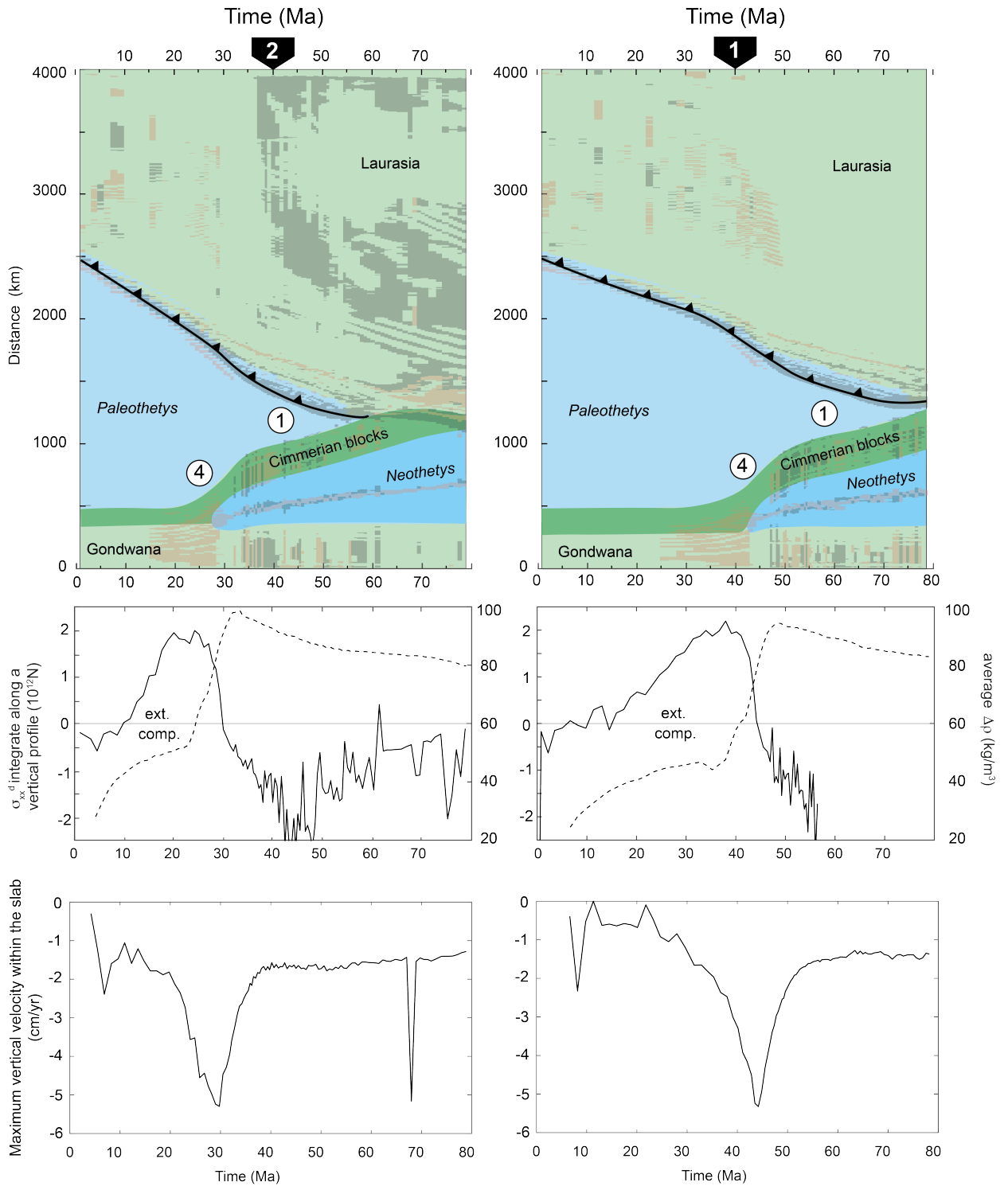


Figure 8: Time evolution of surface transects for two distinct simulations with convergence imposed on the upper plate (respectively 2 and 1 cm/year). Continental and oceanic crust are represented in green and blue, respectively. Tensional and compressional deformation are shown in red and black, respectively. Circled numbers refer to the Cimmerian block drift velocity. Dashed line correspond to the average density contrast between the slab and the mantle. Solid line correspond to the tectonic force recorded within the continent of the lower plate.

subduction zone than with a punctual plume. The latter may nevertheless help strain localization and Neotethys opening, since mantle plumes also trigger the formation of elongated rifts when far-field stresses are prone to rifting (Burov and Gerya, 2014), and might be needed to overcome the basal shear and induce continental breakup when the continental margin moves with respect to the underlying mantle Koptev et al. (2019).

Our models which start after ridge subduction do not include mechanical heterogeneities in the oceanic basin that could localize strain rather than transmit stress to the passive margin. In the case of the Paleotethys, such mechanical heterogeneities, as those introduced by transform faults are supposed to be normal to the trench as paleogeographic reconstruction indicates that the subduction trench was almost parallel to the former ridge. In a different context, the presence of mechanical heterogeneities in the oceanic basin could potentially lead to lower plate oceanic rifting as subduction resume.

The velocity of the Cimmerian block drift, inferred from paleomagnetic data, is about 7-8 cm/year (Muttoni et al., 2009). In our simulations, the drifting velocity of the micro-continent is 4 cm/year when the slab is not anchored in the lower mantle, and then 1 cm/year. Our simulation is nevertheless limited by the impermeable boundary condition imposed between the upper and lower mantle, so that timescales might have been somewhat underestimated here.

Paleomagnetic and geological data advocate for a slow convergence rate between Laurasia and Gondwana, yet with large uncertainties. Since models with positive lower plate velocities do not lead to lower plate rifting (or to rifting but not spreading), as opposed to models with positive upper plate velocities (Figs.5,6), we propose that, in the case of the Cimmerian blocks, Eurasia was likely moving southward relative to the mantle located just below it.

Finally, our study allows investigating the time gap between the subduction of the Paleotethys ridge and the opening of the Neotethys. We find that this depends on the convergence rate and the size of the Paleotethys ocean. The shorter the Paleotethys ocean domain, the less basal shear energy dissipation, and the shorter the time it takes for the slab to reach 410 km depth. The higher the convergence rate, the sooner the slab tip reaches the 410 km phase transition depth, hence the earlier the lower plate continental breakup. The convergence rate, however, also impacts slab dip and the timing to reach 410 km depth: slab dip increases when convergence decreases (Fig. 8), so that the relationship between the amount of convergence and the onset of lower plate continental breakup is not perfectly linear. In our set of simulations, the time gap between ridge subduction and lower plate continental breakup ranges between 20 Ma (for a 2 cm/year imposed convergence) and 70 Ma (for a 0.5 cm/year imposed convergence), which provides an important constraint on paleo-reconstructions, owing to the fact that the timing of Paleotethys ridge subduction

remains highly debated (Stampfli and Borel, 2002; Torsvik et al., 2012). We have shown that a longer ocean may delay subduction initiation and therefore continental breakup (i.e. until the slab reaches the 410 km depth; see Supplementary material), yet that instantaneous ridge subduction and continental breakup, as proposed in some paleogeographic reconstructions, is very unlikely (Fig. 1C).

## 5. Conclusions

We present quantitative slab-drag models for the dislocation of Gondwana based on thermo-mechanical numerical simulations accounting for realistic slab densities and therefore self-consistent slab pull variations during subduction, using a free surface, non-linear temperature dependant flow laws. Our main conclusions are:

1. The marked increase in slab density related to phase transitions in an ocean devoid of active mid-oceanic ridge, in addition to gravitational potential energy of the continental lithosphere, can cause continental rifting in the lower plate.
2. Provided that the lower plate moves at the same velocity as the underlying mantle (i.e. no significant horizontal basal shear is exerted on the continent), slab-drag appears as a viable mechanism for lower plate continental breakup. Additional sources of extensional stress (i.e plume impingement) or preexistent weaknesses within the continental plate may help but are not necessary.
3. On the contrary, if the lower plate moves with respect to the underlying mantle, the necking instability necessary to reach continental breakup stage is strongly hampered by basal shear.
4. Simple models based on Newtonian rheologies and constant density, while valid for studying first order problem in subduction dynamics, are not sufficient to capture continental breakup and can not be used to model slab-drag continental breakup.
5. Contrary to some paleogeographic reconstruction models, continental breakup can not be coeval with ridge subduction: the sinking slab density must first increase by reaching the olivine-wadsleyite transition (410 km). This time lag strongly depends on the length of the subducting ocean, the imposed convergence rate and the dip of the slab.
6. The localisation of the deformation always occurs 100-200 km within the passive margin due to bending stresses and rheological contrasts, thereby promoting the formation of ribbon like micro-continents.
7. The formation and drift of the Cimmerian blocks was likely induced by the slab pull force of the subducted Paleotethys ocean in the context of the slow convergence between Eurasia and Gondwana. Results also suggest that the Paleotethys ridge was subducted long before the opening of the Neotethys.

## 6. Acknowledgements

This work benefited from the financial support of the bilateral cooperation program TRIGGER between France and Iran, led by the CNRS and the Geological Survey of Iran (GSI). The authors thank the MeSU platform of Sorbonne University for the computing time, Fabio Capitanio for reviewing the manuscript and Hans Thybo for his editorial work.

## References

- Agard, P., Omrani, J., Jolivet, L., Whitechurch, H., Vrielynck, B., Spakman, W., Monié, P., Meyer, B., Wortel, R., 2011. Zagros orogeny: a subduction-dominated process. *Geological Magazine* 148, 692–725.
- Arcay, D., Lallemand, S., Doin, M.P., 2008. Back-arc strain in subduction zones: Statistical observations versus numerical modeling. *Geochemistry, Geophysics, Geosystems* 9.
- Artemieva, I.M., 2006. Global  $1 \times 1$  thermal model tc1 for the continental lithosphere: implications for lithosphere secular evolution. *Tectonophysics* 416, 245–277.
- Benilov, E., Naulin, V., Rasmussen, J.J., 2002. Does a sheared flow stabilize inversely stratified fluid? *Physics of Fluids* 14, 1674–1680.
- Brune, S., Williams, S.E., Butterworth, N.P., Müller, R.D., 2016. Abrupt plate accelerations shape rifted continental margins. *Nature* 536, 201–204.
- Buiter, S.J., Pfiffner, O.A., Beaumont, C., 2009. Inversion of extensional sedimentary basins: A numerical evaluation of the localisation of shortening. *Earth and Planetary Science Letters* 288, 492–504.
- Burkett, E.R., Billen, M.I., 2009. Dynamics and implications of slab detachment due to ridge-trench collision. *Journal of Geophysical Research: Solid Earth* 114.
- Burov, E., Gerya, T., 2014. Asymmetric three-dimensional topography over mantle plumes. *Nature* 513, 85–89.
- Burov, E.B., Diament, M., 1995. The effective elastic thickness ( $t_e$ ) of continental lithosphere: What does it really mean? *Journal of Geophysical Research: Solid Earth* 100, 3905–3927.
- Burov, E.B., Guillou-Frottier, L., 1999. Thermomechanical behavior of large ash flow calderas. *Journal of Geophysical Research: Solid Earth* 104, 23081–23109.

- Čížková, H., van den Berg, A.P., Spakman, W., Matyska, C., 2012. The viscosity of earth's lower mantle inferred from sinking speed of subducted lithosphere. *Physics of the earth and Planetary Interiors* 200, 56–62.
- Cloos, M., 1993. Lithospheric buoyancy and collisional orogenesis: Subduction of oceanic plateaus, continental margins, island arcs, spreading ridges, and seamounts. *Geological Society of America Bulletin* 105, 715–737.
- Dal Zilio, L., Faccenda, M., Capitanio, F., 2018. The role of deep subduction in supercontinent breakup. *Tectonophysics* 746, 312–324.
- Faccenda, M., Dal Zilio, L., 2017. The role of solid–solid phase transitions in mantle convection. *Lithos* 268, 198–224.
- Gerya, T.V., Maresch, W.V., Willner, A.P., Van Reenen, D.D., Smit, C.A., 2001. Inherent gravitational instability of thickened continental crust with regionally developed low-to medium-pressure granulite facies metamorphism. *Earth and Planetary Science Letters* 190, 221–235.
- Gerya, T.V., Meilick, F., 2011. Geodynamic regimes of subduction under an active margin: effects of rheological weakening by fluids and melts. *Journal of Metamorphic Geology* 29, 7–31.
- Gerya, T.V., Perchuk, L.L., Maresch, W.V., Willner, A.P., 2004. Inherent gravitational instability of hot continental crust: Implications for doming and diapirism in granulite facies terrains. *SPECIAL PAPERS-GEOLOGICAL SOCIETY OF AMERICA* , 97–116.
- Gleason, G.C., Tullis, J., 1995. A flow law for dislocation creep of quartz aggregates determined with the molten salt cell. *Tectonophysics* 247, 1–23.
- Goes, S., Agrusta, R., van Hunen, J., Garel, F., 2017. Subduction-transition zone interaction: A review. *Geosphere* 13, 644–664.
- Guillou, L., Jaupart, C., 1995. On the effect of continents on mantle convection. *Journal of Geophysical Research: Solid Earth* 100, 24217–24238.
- Heron, P.J., 2019. Mantle plumes and mantle dynamics in the wilson cycle. *Geological Society, London, Special Publications* 470, 87–103.
- Heuret, A., 2005. Dynamique des zones de subduction: étude statistique globale et approche analogique. Ph.D. thesis. Université Montpellier II-Sciences et Techniques du Languedoc.

- Heuret, A., Funiciello, F., Faccenna, C., Lallemand, S., 2007. Plate kinematics, slab shape and back-arc stress: a comparison between laboratory models and current subduction zones. *Earth and Planetary Science Letters* 256, 473–483.
- Heuret, A., Lallemand, S., 2005. Plate motions, slab dynamics and back-arc deformation. *Physics of the Earth and Planetary Interiors* 149, 31–51.
- Huismans, R.S., Podladchikov, Y.Y., Cloetingh, S., 2001. Transition from passive to active rifting: Relative importance of asthenospheric doming and passive extension of the lithosphere. *Journal of Geophysical Research: Solid Earth* 106, 11271–11291.
- van Hunen, J., van den Berg, A.P., Vlaar, N.J., 2000. A thermo-mechanical model of horizontal subduction below an overriding plate. *Earth and Planetary Science Letters* 182, 157–169.
- van Hunen, J., Huang, J., Zhong, S., 2003. The effect of shearing on the onset and vigor of small-scale convection in a newtonian rheology. *Geophysical research letters* 30.
- Jolivet, L., Faccenna, C., Agard, P., Frizon de Lamotte, D., Menant, A., Sternai, P., Guillocheau, F., 2016. Neo-tethys geodynamics and mantle convection: from extension to compression in africa and a conceptual model for obduction. *Canadian journal of earth sciences* 53, 1190–1204.
- Jourdon, A., Le Pourhiet, L., Mouthereau, F., May, D., 2020. Modes of propagation of continental break-up and associated oblique rift structures. *Journal of Geophysical Research: Solid Earth* , e2020JB019906.
- Jourdon, A., Le Pourhiet, L., Petit, C., Rolland, Y., 2018. Impact of range-parallel sediment transport on 2d thermo-mechanical models of mountain belts: Application to the kyrgyz tien shan. *Terra Nova* 30, 279–288.
- Koptev, A., Beniest, A., Gerya, T., Ehlers, T.A., Jolivet, L., Leroy, S., 2019. Plume-induced breakup of a subducting plate: Microcontinent formation without cessation of the subduction process. *Geophysical Research Letters* 46, 3663–3675.
- Lallemand, S., Heuret, A., Faccenna, C., Funiciello, F., 2008. Subduction dynamics as revealed by trench migration. *Tectonics* 27.
- Lavecchia, A., Thieulot, C., Beekman, F., Cloetingh, S., Clark, S., 2017. Lithosphere erosion and continental breakup: Interaction of extension, plume upwelling and melting. *Earth and Planetary Science Letters* 467, 89–98.

- Le Pourhiet, L., Chamot-Rooke, N., Delescluse, M., May, D.A., Watremez, L., Pubellier, M., 2018. Continental break-up of the south china sea stalled by far-field compression. *Nature Geoscience* 11, 605–609.
- May, D.A., Brown, J., Le Pourhiet, L., 2014. ptatin3d: High-performance methods for long-term lithospheric dynamics, in: *Proceedings of the international conference for high performance computing, networking, storage and analysis*, IEEE Press. pp. 274–284.
- May, D.A., Brown, J., Le Pourhiet, L., 2015. A scalable, matrix-free multigrid preconditioner for finite element discretizations of heterogeneous stokes flow. *Computer Methods in Applied Mechanics and Engineering* 290, 496–523.
- Muttoni, G., Mattei, M., Balini, M., Zanchi, A., Gaetani, M., Berra, F., 2009. The drift history of iran from the ordovician to the triassic. *Geological Society, London, Special Publications* 312, 7–29.
- Müller, R.D., Gaina, C., Roest, W.R., Hansen, D.L., 2001. A recipe for microcontinent formation. *Geology* 29, 203–206.
- Ranalli, G., Murphy, D.C., 1987. Rheological stratification of the lithosphere. *Tectonophysics* 132, 281–295.
- Ricou, L.E., 1994. Tethys reconstructed: plates, continental fragments and their boundaries since 260 ma from central america to south-eastern asia. *Geodinamica acta* 7, 169–218.
- Schellart, W., 2004. Quantifying the net slab pull force as a driving mechanism for plate tectonics. *Geophysical research letters* 31.
- Smith, R.B., 1977. Formation of folds, boudinage, and mullions in non-newtonian materials. *Geological Society of America Bulletin* 88, 312–320.
- Stampfli, G.M., Borel, G., 2002. A plate tectonic model for the paleozoic and mesozoic constrained by dynamic plate boundaries and restored synthetic oceanic isochrons. *Earth and Planetary Science Letters* 196, 17–33.
- Stüwe, K., et al., 2002. *Geodynamics of the Lithosphere*. Springer.
- Torsvik, T.H., Cocks, L.R.M., 2016. *Earth history and palaeogeography*. Cambridge University Press.

- Torsvik, T.H., Van der Voo, R., Preeden, U., Mac Niocaill, C., Steinberger, B., Doubrovine, P.V., Van Hinsbergen, D.J., Domeier, M., Gaina, C., Tohver, E., et al., 2012. Phanerozoic polar wander, palaeogeography and dynamics. *Earth-Science Reviews* 114, 325–368.
- Turcotte, D.L., Schubert, G., 2014. *Geodynamics*. Cambridge university press.
- Vasilyev, O.V., Gerya, T.V., Yuen, D.A., 2004. The application of multidimensional wavelets to unveiling multi-phase diagrams and in situ physical properties of rocks. *Earth and Planetary Science Letters* 223, 49–64.
- Wan, B., Chu, Y., Chen, L., Liang, X., Zhang, Z., Ao, S., Talebian, M., 2021. Paleotethys subduction induced slab-drag opening the neo-tethys: Evidence from an iranian segment of gondwana. *Earth-Science Reviews* 221, 103788.
- Wan, B., Wu, F., Chen, L., Zhao, L., Liang, X., Xiao, W., Zhu, R., 2019. Cyclical one-way continental rupture-drift in the tethyan evolution: Subduction-driven plate tectonics. *Science China Earth Sciences* 62, 2005–2016.
- Wolf, S.G., Huisman, R.S., 2019. Mountain building or backarc extension in ocean-continent subduction systems: A function of backarc lithospheric strength and absolute plate velocities. *Journal of Geophysical Research: Solid Earth* 124, 7461–7482.
- Yan, Y., Zhao, Q., Zhang, Y., Huang, B., Zheng, W., Zhang, P., 2019. Direct paleomagnetic constraint on the closure of paleo-tethys and its implications for linking the tibetan and southeast asian blocks. *Geophysical Research Letters* 46, 14368–14376.
- Yang, S., Li, Z.H., Wan, B., Chen, L., Kaus, B.J., 2021. Subduction-induced back-arc extension versus far-field stretching: Contrasting modes for continental marginal break-up. *Geochemistry, Geophysics, Geosystems* 22, e2020GC009416.